Nanoscale

ARTICLE

Microstructural transitions in resistive random access memory composed of molybdenum oxide with copper during switching cycles

Received 00th January 20xx,
Accepted 00th January 20xx

DOI: 10.1039/x0xx00000x

www.rsc.org/

Masashi Arita,* Yuuki Ohno, Yosuke Murakami, Keisuke Takamizawa, Atsushi Tsurumaki-Fukuchi and Yasuo Takahashi

The switching operation of a Cu/MoO_x/TiN resistive random access memory (ReRAM) device was investigated using in situ transmission electron microscopy (TEM), where the TiN surface was slightly oxidized (ox-TiN). The relationship between the switching properties and the dynamics of the ReRAM microstructure was confirmed experimentally. The growth and/or shrinkage of the conductive filament (CF) can be classified into two set modes and two reset modes. These switching modes depend on the device's switching history, factors such as the amount of Cu inclusions in the MoO_x layer, and the CF geometry. High currents are required to produce an observable change in the CF. However, sharp and stable switching behaviour can be achieved without requiring such a major change. The local region around the CF is thought to contribute to the ReRAM switching process.

Since the pioneering works on resistive random access memories (ReRAMs) were performed around the year 2000,[1–3] vast numbers of works have been reported in this field, as described in numerous review articles.[4–13] This is occurring because the ReRAM shows strong potential for use as a next-generation memory; it offers a simple device structure that would be advantageous for integration, a high on/off ratio, and nonvolatility. In addition to binary operation, analogue memory operations that can be used for artificial neural network hardware have been investigated energetically in recent years.[14–17] Application of a voltage to a ReRAM device, where the ReRAM material is sandwiched between two electrodes to form a simple capacitor structure, causes the device resistance to switch between the high resistance state (HRS) and the low resistance state (LRS) (and intermediate states in some cases). This switching process can be used for the memory operation. The ReRAM materials reported to date can be categorized into three groups: perovskite-type oxides, binary oxides and solid electrolytes (SE; e.g., chalcogenides or oxides). The ReRAMs that are based on the latter two material groups are considered to operate according to an electrochemical mechanism, by which a conductive filament (CF) is formed in the ReRAM material, while the electronic state at the electrode-oxide interface plays an important role in the perovskite-type ReRAM.[11,12] The SE material is usually sandwiched between an electrochemically active electrode (e.g., copper (Cu) or silver (Ag)) and an inactive electrode (e.g., platinum (Pt) or titanium nitride (TiN)).[18–28] The resistance switching is considered to occur because of the formation and rupture (or shrinkage) of CFs composed of Cu (or Ag), and this type of ReRAM is called the conductive bridge RAM (CBRAM). The molybdenum oxide (MoO_x)-based device with the Cu electrode investigated in this report is a type of CBRAM,[29] while MoO_x shows ReRAM switching behaviour even without the Cu electrode.[30]

Here, the ReRAM operation of the Cu/MoO_x/TiN structure is briefly described based on the assumption of the conventional electrochemical model for the CBRAM,[6,8,12,13] where Cu is the active top electrode (TE) and TiN is the inactive bottom electrode (BE). Application of a positive voltage to the Cu TE induces oxidation of the Cu to produce cations. These cations move along the electric field toward the BE and are metallized at the BE to form a CF. The CF grows towards the TE, and the resistance reaches the LRS when the CF connects the two electrodes. This is called the set process. With reversal of the applied voltage, the opposite reaction occurs, and the CF is ruptured. The resistance then switches to the HRS. This is called the reset process. While this electrochemical model offers a plausible explanation of the switching mechanism of the CBRAM, other factors such as Joule heating caused by the current flow,[31–33] moisture in the atmosphere[34] and the mobility of the ions in the switching layer[35,36] must also be taken into consideration. However, the details of the process are still indistinct, especially when we consider the switching of a realistic CBRAM device, where sufficient switching power must be injected to maintain the LRS (i.e., for memory retention).

Graduate School of Information Science and Technology, Hokkaido University, Sapporo 060-0814, Japan.
* arita@nano.ist.hokudai.ac.jp
† Electronic Supplementary Information (ESI) available: See DOI: 10.1039/x0xx00000x

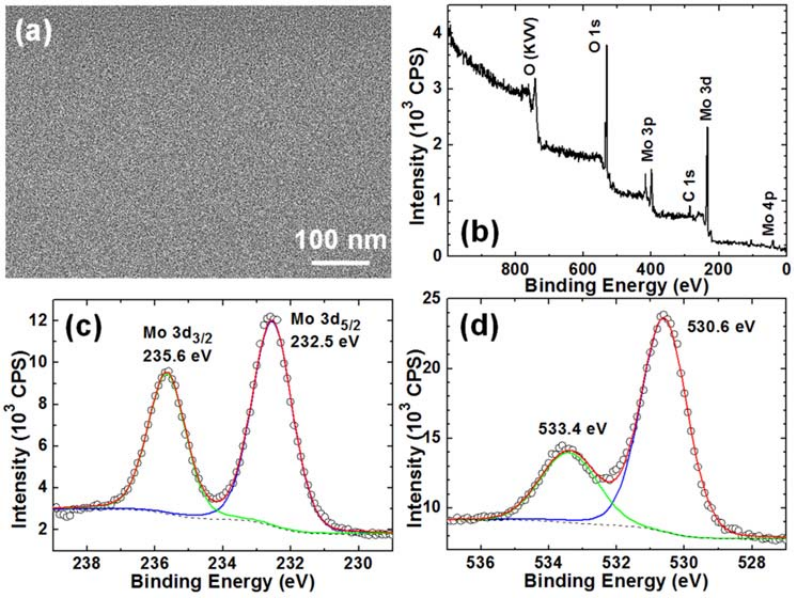

Fig. 1 (a) SEM image and (b)–(d) XPS spectra of the MoO_x film prepared by reactive sputtering of metallic Mo in an Ar-O_2 (20%) atmosphere. Open circles denote measured data, and the red curves are analysis results composed of the two peaks (blue and green curves) and the Shirley-type background (broken curve).

The in situ transmission electron microscopy (in situ TEM) method is used to investigate ReRAM switching in real space, where the geometrical evolution in the ReRAM device can be observed during the switching operation. In addition to perovskite-type ReRAMs[37–39] and devices based on binary oxides,[40–46] many reports on CBRAMs have appeared in recent years. [47–53] In one example, the dynamic growth and rupture of a Cu CF was confirmed during a switching cycle.[47,51] In another report, the CF growth scheme was investigated in detail in terms of its dependence on cation mobility.[35,49] The majority of these works have focused on the CF growth mechanism based on the electrochemistry of the process. When the set/reset switching of realistic CBRAM devices is considered in addition to these fundamental electrochemical studies, sequential switching cycles should be executed using stacked ReRAM samples. Recently, Kudo et al.[54] performed cyclic current-voltage (*I-V)* switching and pulse switching operations on miniaturized CuTe/insulator CBRAM devices for in situ TEM, realizing long retention (3 months) and good endurance (10^5 cycles), and also discussed CF formation in the insulator with increasing switching current. Works in this category remain quite rare (particularly works on the reset process), while there are also other works that study cyclic ReRAM switching.[55,56]

In this work, we performed multiple set/reset cycles of a Cu/MoO_x/TiN CBRAM device using in situ TEM, and the details of the CF evolution were observed. As a result, we found that there were two set modes and two reset modes where the CF appeared/disappeared in the MoO_x layer, depending on the device switching history. An observable change in the CF geometry in MoO_x was detected under high currents. However, sharp and stable operation was achieved without the need for such large changes.

Results and discussion

Characterization of MoO_x film

The MoO_x film, which was prepared by reactive sputtering, had a smooth surface, as shown in the scanning electron microscopy (SEM) image (Fig. 1(a)). X-ray photoelectron spectroscopy (XPS) data are presented in Fig. 1(b)–(d) that show the chemical state of the film. The wide-scan spectrum was composed of the Mo and O peaks (Fig. 1(b)). The peak assigned as C 1s came from surface contamination, which can be used as a reference value (284.6 eV) to correct the peak shift caused by the charge-up of the specimen. The narrow-scan spectrum shown in Fig. 1(c) is for Mo 3d. There are two peaks for Mo $3d_{5/2}$ (232.5 eV) and Mo $3d_{3/2}$ (235.6 eV). These values correspond well with those given for Mo^{6+} in previous reports[57–59] (e.g., 232.5 and 235.6 eV, respectively[59]). The ratio of integrated intensity between these peaks was reasonable ($3d_{5/2}$:$3d_{3/2}$ = 3:2). The O 1s spectrum shown in Fig. 1(d) comprises two peaks at 530.6 eV and 533.4 eV, where the former peak is thought to come from the molybdenum oxide while the latter is believed to come from the adsorbate (O^{2-}, OH^- or H_2O).[59] Therefore, the chemical state of the fabricated molybdenum oxide was concluded to be quite similar to that of MoO_3.

Figure 2 shows the θ–2θ X-ray diffraction (XRD) patterns of the as-deposited and heat-treated films. The as-deposited film showed no diffraction peaks, and this indicates that the MoO_x studied here was amorphous. This amorphous state was maintained at 300°C for 10 min in air. Crystallization to β-MoO_3 began at 400°C, and the α-MoO_3 peaks appeared at 500°C. This tendency was same as an earlier report.[60] While

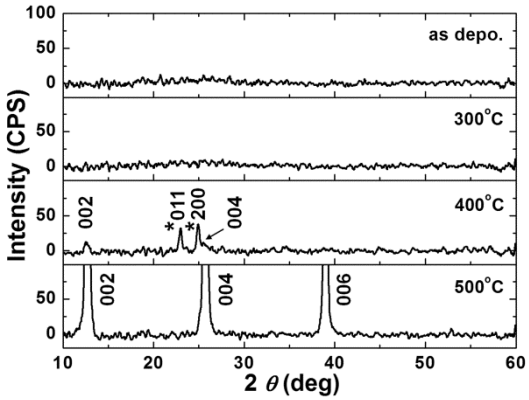

Fig. 2 XRD patterns of MoO_x films, where the background signals from the SiO_2/Si substrates were subtracted. The as-deposited film and the films after heat treatment in air at 300, 400 and 500°C (10 min) are compared. Crystallization began at 400°C, and a clear preferential orientation of MoO_3 along [001] was identified at 500°C. Reflection indices with asterisks are of β-MoO_3, and the others are of α-MoO_3.

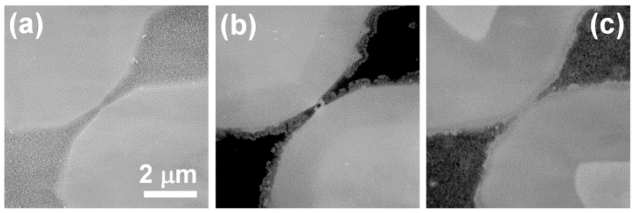

Fig. 3 TEM images of the Cu pattern (a) before and (b) a few days after deposition of the MoO_x layer. (c) TEM image 1 month after MoO_x deposition. The region showing dark contrast near the pattern expanded, indicating Cu dissolution into MoO_x. The image contrast was individually enhanced to clarify the faint contrast.

both lithography and TEM sample preparation processes may increase the specimen temperature, it was still thought to be lower than 400°C. Therefore, the specimen must be in an amorphous state during the electronic measurements.

To check the degree of Cu dissolution into the MoO_x film, Cu patterns were formed on a Si_3N_4 membrane for TEM observation. The experimental details of this process can be seen in our earlier report.[61] One example is shown in Fig. 3(a), where the dark region corresponds to the Cu pattern, while the other region is the Si_3N_4 membrane. After TEM observation, a 30-nm-thick MoO_x layer was deposited to cover the Cu electrode. Figure 3(b) shows a TEM image that was acquired a few days after this deposition process without application of a voltage. Note that the image contrast was enhanced to identify the faint contrast that is visible around the Cu pattern edge. The pattern edge became rougher, and the contrast in the region within a distance of approximately 1.2 μm from the pattern edge became darker. This tendency can be seen clearly in Fig. 3(c), where the sample had been kept in a vacuum (~1 Pa) at room temperature (RT) for 1 month after the deposition process without any voltage application. The Cu edge retreated, the region near the edge became darker, and this region expanded to a width of approximately 3 μm. This result indicates that the Cu tends to be dissolved into MoO_x prepared by reactive sputtering, and that MoO_x can act as a solid electrolyte like GeS.[8,19] The MoO_x layer can be described as Cu:MoO_x[62] though the notation of MoO_x is used throughout this report.

Switching properties of reference device

Reference devices with conventional ReRAM structures (Pt/Cu/MoO_x on TiN inside SiO_2 contact holes) were fabricated

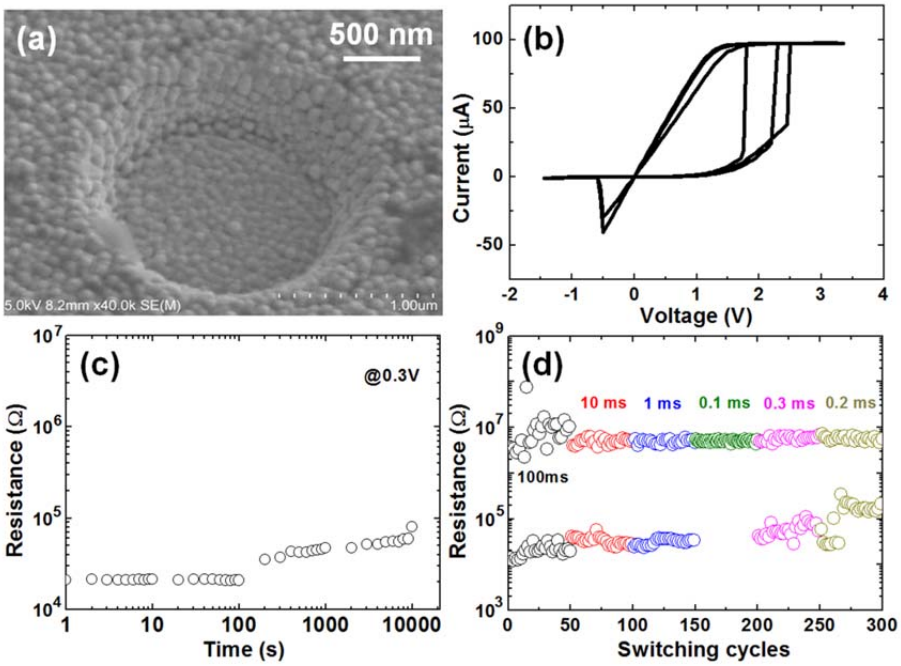

Fig. 4 (a) SEM image of a typical ReRAM device, (b) bipolar *I-V* switching curve, (c) LRS retention curve measured at 0.3 V, and (d) endurance properties using voltage pulses of ±2 V with widths of between 0.1 and 100 ms.

to verify the fundamental properties of our Cu/MoO_x structure. One example is shown in Fig. 4(a), where the device was 2 μm in diameter, while the major device size is 4 or 8 μm in the present work. Full details of the fabrication process and the electrical measurements will be given in the "Methods" section. As described there, the TiN surface was treated using O_2 plasma, and its surface was expected to be slightly oxidized (ox-TiN), as reported earlier.[56] Therefore, the actual ReRAM stack can be described as Pt/Cu/MoO_x/ox-TiN/TiN. A typical *I-V* graph of the reference device is shown in Fig. 4(b), where three successive switching curves are superposed. As the voltage increased, the current jumped abruptly at around 2 V to reach the compliance current I_{comp} (or the limitation current). The resistance changed from >10 MΩ (HRS) to ~15 kΩ (LRS); these states were evaluated using the currents at 0.3 V. Reset switching occurred at −0.5 V, where the resistance recovered to the HRS. This is the typical bipolar switching behaviour of CBRAMs. An example of the LRS retention property is shown in Fig. 4(c), which was measured at RT. The LRS was maintained for at least 3 h, although the resistance increased gradually after 100 s. However, this time period is long enough for the TEM experiments. The retention time is expected to be elongated by increasing the set current.[54] Figure 4(d) shows an example of the pulse endurance graph using ±2 V pulses while changing the pulse width. When the pulse width was reduced from 100 ms to 100 μs, the pulse switching was not realized. Afterwards, it was elongated to 300 μs, and the switching recovered. The resistance ratio of HRS/LRS was more than 50 when pulses longer than 100 μs were used. Though this switching speed was not as quick as that of a real ReRAM device, it may be improved by optimization of the device structure, e.g., the MoO_x thickness. These results for the Cu/MoO_x reference devices reflect the typical switching characteristics of CBRAMs.[6,13] Therefore, the in situ TEM results that are described in the next section are expected to provide useful information to aid in understanding of the switching operation of CBRAMs.

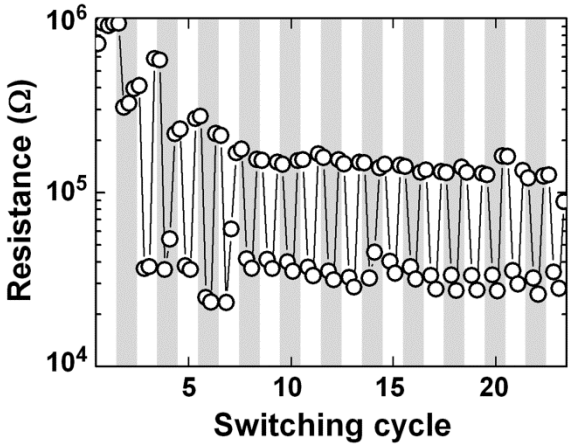

Fig. 5 (Example 1) Cyclic endurance properties obtained from *I-V* switching curves, where the resistance was evaluated at ±0.3 V for the forward and backward voltage sweeps. There are four data points for each cycle. Note that the evaluated resistance include that of the TiN/Si BE.

Cyclic in situ TEM

In this section, two sets of in situ TEM results are presented; both sets of results were measured using ReRAMs with Pt/Cu/MoO_x(50 nm)/ox-TiN/TiN structures. The ReRAM was nearly circular, with a diameter of approximately 350 nm. In both cases, multiple *I-V* switching cycles were realized, and the microstructural evolution during the ReRAM switching operation was observed. The resistance values given in the following paragraphs were estimated at +0.3 V and/or −0.3 V using the *I-V* curves. As described in the "Methods" section, the electronic measurements were performed through TiN/Si which showed the non-linear *I-V* character. This must be the main reason of the non-linear *I-V* graphs for the LRS shown in this subsection. The actual LRS resistance of the ReRAM is thought to be lower than the values shown below.

Example 1: In this example, 23 continuous *I-V* cycles were investigated using TEM while expanding the voltage range (from ±1.0 to ±2.2 V) and increasing I_{comp} (from 50 to 120 μA). The cyclic endurance graph is shown in Fig. 5. While no resistance change occurred during the first cycle, the ReRAM switching window was open during the repetition of the *I-V* cycles. Correspondingly, the Cu filament grew in the MoO_x layer. The filament shrank considerably at the 23rd cycle, and the resistance switching behaviour then became unstable. Details of this behaviour will be given in the following paragraphs and are also provi

ded in an electronic supplementary information file (ESI_1.wmv).

Three *I-V* curves from the initial state are shown in Fig. 6(a). In the first cycle with the voltage range of ±1.0 V, no resistance hysteresis was observed, and there was no change in the TEM video image. The processes using positive or negative voltages

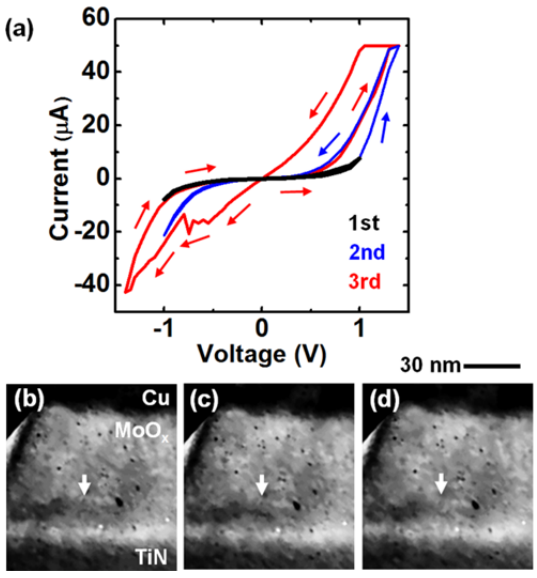

Fig. 6 (Example 1) (a) First to third *I-V* curves from the initial state. Arrows indicate the direction of the voltage sweep. The images were extracted from the video of the third cycle; (b) before and (c) after the set cycle, and (d) after the reset cycle. The growth and shrinkage of the Cu deposit is identified (and indicated by arrows). The clear dark dots were due to dust and/or cell imperfections in our TEM video camera.

will be called the set or reset processes (or cycles) in this report, even if there is no clear set or reset switching. In the second cycle, with its maximum voltage of +1.4 V, a weak hysteretic property was identified in the set process. According to the electrochemical model,[6,8,12,13] Cu is believed to be dissolved, and subsequently drifts in the MoO_x layer to the BE, where it forms deposits. However, no change was seen in the TEM image. In the negative voltage region, there was no reset switching, while the resistance was lower than that in the first cycle. In the third cycle, the forward curve in the set process fitted the backward curve of the second set cycle. This indicates that a slightly lower resistance value (400 kΩ) than that of the initial state (700 kΩ) was maintained. The resistance was much reduced (approximately 30 kΩ including the resistance of TiN/Si) in the third set process. Under a negative applied voltage, the resistance increased at around −0.6 V and followed the blue curve of the second cycle. The resistance increased further at around −1.2 V with subsequent voltage applications (and thus negative current flows), and the resistance nearly recovered to its initial value. In this cycle, where there is a clear hysteresis window, a slight contrast change was identified in the TEM video, as shown in Fig. 6(b)–(d). A video image that was acquired just before the third cycle is presented in Fig. 6(b), where the horizontally-aligned bright area on the TiN BE corresponds to ox-TiN. There was also a region with dark contrast near the MoO_x/ox-TiN/TiN interface, which may correspond to the region of a Cu deposit, as reported earlier.[47,53] This was also observed in the initial state. In an earlier work, heat treatment of a Cu/SiO_2/BE structure was reported to induce Cu segregation at the SiO_2/BE interface.[63] A similar phenomenon may occur here, caused by possible temperature increases during TEM sample preparation by ion milling. Thus, Cu dissolution into MoO_x is expected in this sample even before the *I-V* operation starts, and this may influence both the initial resistance and the microstructural evolution during ReRAM operation. After the set cycle with a positive voltage, the Cu deposit grew at the position indicated by the arrow (Fig. 6(c)). The deposit disappeared after the reset cycle with a negative voltage (Fig. 6(d)). This Cu deposit must therefore play an important role in the ReRAM switching process. These processes are used for device initialization, although there was no abrupt current jump (or forming) observed in many valence change memory (VCM)-type ReRAMs, where the oxygen vacancies contribute to the resistance switching. Clear and abrupt current jumps (and thus resistance changes) began after the 4th and 5th cycles.

The set/reset operation in the 6th cycle is shown in Fig. 7, where the *I-V* curve (Fig. 7(a)) and the corresponding TEM video images (Fig. 7(b)–(g) for set and Fig. 7(h)–(m) for reset) are compared. In Fig. 7(b), which shows an image taken just after the start of this cycle, a Cu deposit with a round contrast is identified at the centre-bottom of the MoO_x layer; this deposit grew in the 5th cycle. In the *I-V* curve, an abrupt current increase that corresponds to set switching is identified at +1.15 V (states c and d). The deposit did not show a clear morphological change in the TEM image at this stage (Fig. 7(c)–(d)). It then grew from the BE to the TE, as shown in Fig. 7(e)–(g) with continuous voltage application and current flow after the set switching process. This additional process, which is used to enhance the deposit growth, is called the over-set in this report. The resulting deposit did not bridge the gap between the TE and the BE at this stage, although the resistance was reduced much. In the negative voltage region of the *I-V* graph, a clear current reduction corresponding to reset switching occurred between −0.7 V and −0.8 V (states j and k). The filament that appeared before reset switching (Fig. 7(h)–(j)) shrank only very slightly with this reset switching behaviour (Fig. 7(k)). With continuing current flow, the deposit shrank further toward the BE giving roundish contrast (Fig. 7(l)-(m)), although the shrinkage at this stage was small. This additional process, which is used to reduce a deposit, is called the over-reset in this report. The deposit grew and shrank according to the current flow. Thus, this deposit seems to work as the CF,

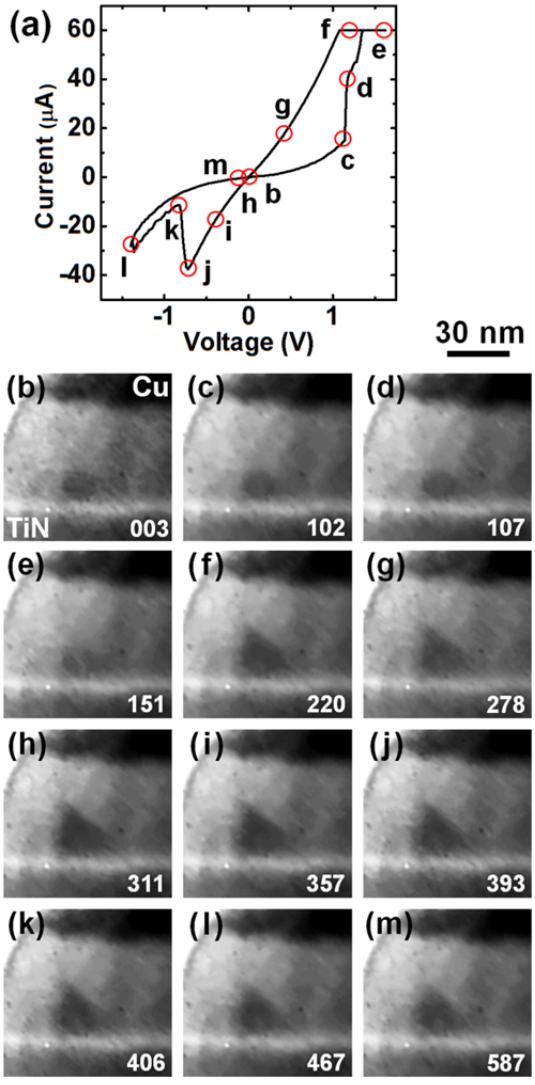

Fig. 7 (Example 1) Set/reset operation of the 6th cycle. (a) *I-V* switching curve and corresponding TEM video images of the (b–g) set and (h–m) reset processes. The number shown in each photograph is the video frame number, and the frame interval was 30 ms.

even though it did not show a clear morphological change at the abrupt set/reset switching moment. The growth and shrinkage scheme observed here fits the behaviour of the filament models reported to date.[6,8,12,13] However, the CF in MoO_x does not need to bridge the TE and the BE to realize a resistance reduction.

To investigate the CF growth in successive cycles, the over-set process was gradually strengthened with increasing I_{comp} while the voltage range remained constant. Here, to prevent CF shrinkage, almost no over-reset operation was introduced. Figure 8(a) shows the 9th to 13th set/reset cycles with increasing maximum positive current. The set voltage was approximately 1.4 V without any systematic change. The reset voltage was approximately −1.1 V. The resistance gradually decreased over time from the 9th to the 13th cycle. Corresponding TEM images acquired after each set operation are presented as Fig. 8(b)–(f). The CF at the centre of the image grew step-by-step from the BE to the TE. While the CF contacted to the Cu TE in Fig. 8(f), the corresponding LRS did not show dramatic current increase (13th cycle in Fig. 8(a)). This is because the TiN/Si BE serially connected to the switching layers limited the current as described in the first part of this subsection. A stable switching cycle could be produced using an operation without a strong over-reset process. An example of such a cycle is shown in Fig. 9, where six successive switching cycles are superposed. In all cycles, the set switching occurred at +1.5 V, and the reset switching occurred at −1.1±0.1 V. The TEM images (which are not provided here) indicated that the overall CF morphology was maintained during these cycles, while the contrast inside the CF was modulated.

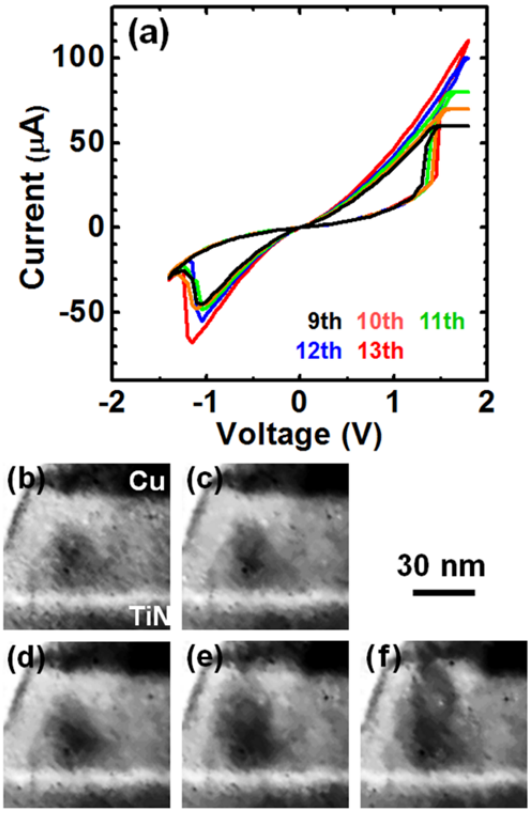

Fig. 8 (Example 1) Set/reset operations from the 9th to the 13th cycle. (a) *I-V* switching curve and corresponding TEM video images after the set processes of the (b) 9th, (c) 10th, (d) 11th, (e) 12th and (f) 13th cycles.

Stable switching cycles can be fatally damaged by a strong over-reset. Figure 10(a) shows a switching curve in the 22nd cycle, and the corresponding images acquired during the reset process are shown in Fig. 10(b)–(f). With increasing negative voltage, reset switching occurred at −1.1 V, as in the previous cycles (Fig. 9). At this instant (i.e., state c), there was no clear change in the CF, as described above. The CF was thinned

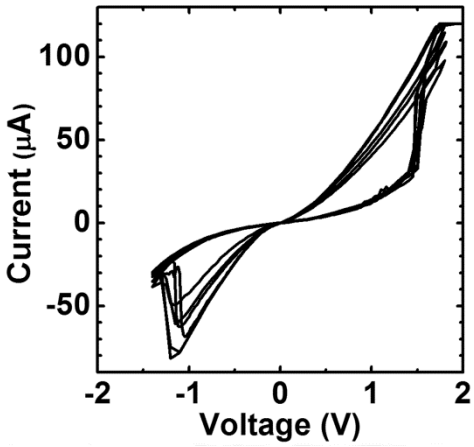

Fig. 9 (Example 1) Six successive set/reset curves without over-reset (14th to 19th cycles).

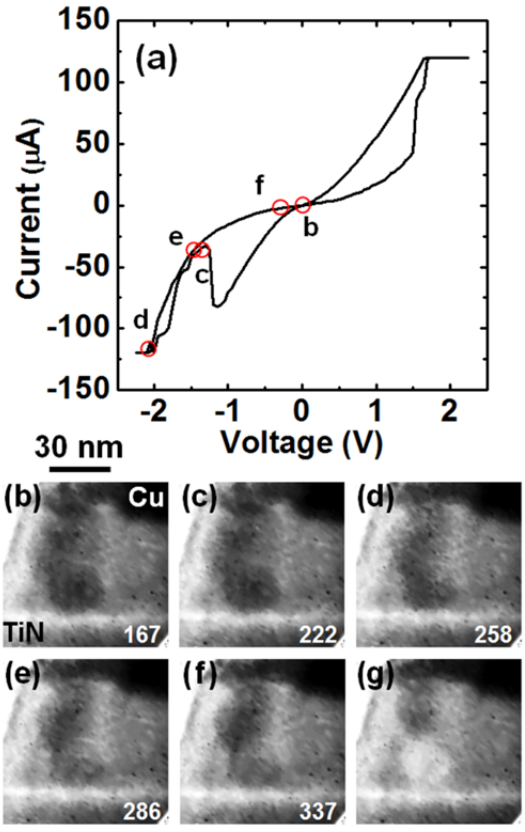

Fig. 10 (Example 1) (a) Switching curve of the 22nd cycle with over-reset, and (b–f) corresponding video images showing the CF shrinkage. The number in each photograph is the video frame number (frame interval of 30 ms). (g) Video image after the 23rd set/reset cycle showing clear rupturing of the CF.

during the over-reset procedure (state d), and the contrast in the lower part became indistinct at states d, e and f. This can be seen more clearly in Fig. 10(g), which was taken after the 23rd set/reset cycle with over-reset. In the area below the residual CF, the contrast is brighter than the other MoO_x region. Because the MoO_x layer is thought to contain Cu after many switching cycles, this contrast difference may be caused by removal of Cu from the CF region during strong over-reset. This indicates that the CF was broken in the lower part due to the current concentration at the CF. The CF that is bridging the TE and the BE appears to be ruptured near the BE, which differs from the phenomenon that occurred in the nonbridging CF (Fig. 7). To clarify the assumption made here, another example of set/reset switching under higher power operation will be discussed in the next paragraphs.

In the discussion here (and in Example 2 described below), change of filamentary contrast in the TEM images are considered with assuming that the darker contrast in the MoO_x layer contained much Cu. To check this assumption, we performed energy dispersive X-ray spectroscopy (EDX) at regions with/without the CF. It was experimentally confirmed that the CF contained much Cu as shown in an electronic supplementary information file (ESI_3.docx). Similar confirmation has been done in our previous works on other CBRAMs.[47,51,56]

Example 2: The device size was the same as that used in Example 1. The initial resistance was approximately 40 MΩ, and thus the initial Cu inclusion level in MoO_x was thought to be much less than that in Example 1. There were 15 positive or negative cycles before set switching occurred, and the resistance decreased to 500 kΩ. This treatment is assessed as being the initialization process of the CBRAM, and these cycles will be excluded from the cycle numbers in the discussion below. After this point, clear set/reset switching began to be observed. In all cases, a higher current was used to generate a thick CF, and a strong over-reset was introduced to enable CF shrinkage to be observed clearly. Details of three successive switching cycles are described in the following paragraphs and are shown in an electronic supplementary information file (ESI_2.wmv).

Figure 11 shows the first set/reset cycle with an I_{comp} of 200 μA, where the *I-V* graph (Fig. 11(a)) and the TEM video images (Fig. 11(b)–(m)) are compared. Here, the region on the right of the image with the grey contrast is thought to be unrelated to the switching because it did not show any change of note during the switching process. With increasing voltage from state b (Fig. 11(b)), the current increased gradually, and a slight change in the middle of the MoO_x layer was seen in state c (Fig. 11(c)). When the voltage reached 3 V, the current increased greatly (state d). Correspondingly, a dark contrast appeared abruptly in the wide area from the TE (around the centre-top of the MoO_x layer), and is thought to be Cu (Fig. 11(d)). Subsequently, this area corrugated to show a clear darker contrast and connected the TE and the BE (Fig. 11(e)–(f)). While the growth direction from the TE differs from that shown in Example 1, this behaviour has been observed in other material systems such as $Ag/SiO_2/Pt$[49] and Ag(or Cu)/ZrO_2/Pt.[50] During the over-set process, the CF grew further and changed its contact position with the TE toward the left in the image (Fig. 11(g)), as clearly shown in the video ESI_2.wmv. Even after bridging between the TE and the BE, the CF shape continued to change. This is important when we consider the realistic use of ReRAM devices in memory applications. In this set process, the resistance changed from 500 kΩ to 8 kΩ. The reset cycle began when 5 min had passed after the set cycle. Note here that the TEM imaging conditions for the reset cycle (Fig. 11(h)–(m)) were slightly different from those used for the set cycle. With increasing negative voltage from state h, the reset switching that increased the resistance by eight times occurred at −1 V (states i and j). During this operation, no clear change was observed in the CF contrast (Fig. 11(h)–(j)). The *I-V* curve then became unstable during the over-reset procedure, and the negative current increased and decreased sharply at states k, l and m. The lower part of the CF vanished from the TEM images when the negative current increased heavily (near the centre-bottom of the MoO_x layer in Fig. 11(k)–(m)). This erasure process is the same as the process that was shown in Fig. 10. In this reset cycle (including the over-reset process), the resistance recovered from 8 kΩ to 300 kΩ. Even after the reset cycle, the Cu content around the first CF must be higher than that in the initial state, as reported previously.[51]

The data from the second set/reset cycle are shown in Fig. 12, where the compliance current was raised to I_{comp} = 400 μA. A detailed discussion of this second switching cycle has already been undertaken in our previous report.[53] In this report, therefore, only a brief explanation will be given for comparison with the other switching cycles. Starting from state b, the set switching occurred at around +2.3 V (states c and d). At this instant, there was no dramatic change in the TEM images (Fig. 12(b)–(e)). When the current increased rapidly (state e), a small dark contrast area corresponding to the CF nucleus appeared near the TiN BE (almost left-end of Fig. 12(e)). This contrast grew towards the Cu TE with increasing current (states f and g, Fig. 12(f) and (g), respectively), and a 35-nm-thick CF that bound the TE and the BE was formed. The resistance decreased from 750 kΩ to 8 kΩ. This CF growth was in the opposite direction to that shown in Fig. 11, but was the same as the growth direction in Example 1. In the reset process, starting from state h, there were two occurrences of weak reset switching before and after state i. However, no clear change in the CF image could be identified (Fig. 12(h)–(j)). A dramatic image change was observed during the over-reset process (states k and l). In Fig. 12(k), the lower part of the CF was ruptured, as shown in Figs. 10 and 11. Subsequently, the CF shrank towards the TE (Fig. 12(l)), and very much disappeared at state m (Fig. 12(m)). The resistance then changed from 9 kΩ to 200 kΩ.

In the third set/reset cycle (I_{comp} = 400 μA), the CF position changed again toward the right (Fig. 13). This is probably due to the strong CF erasure that occurred in the second cycle. While the set switching process was not so sharp, the current gradually increased in the voltage region above 2 V (states c and d of Fig. 13(a)). However, there was no clear contrast change in the TEM images (Fig. 13(b)–(d)). The rate of current

increase became high around state e, and a Cu deposit began to appear at the right-bottom corner of Fig. 13(e). During the over-set process, it grew from the BE to the TE and formed the cone-shaped CF shown in Fig. 13(f) and (g). In this case, a pothole was formed in the Cu TE just above the CF. Because the CF in this cycle formed near the device edge, it was not possible for sufficient Cu to be supplied from the Cu TE. Because of this, the contact between the CF and the Cu TE did not look good. The resistance changed from 160 kΩ to 8 kΩ. The reset cycle began 5 min after the set cycle, and the LRS was maintained during this interval. Reset switching occurred at −1.5 V, but there were no changes of note in the TEM images (Fig. 13(h) and (i)), as observed in the first and second reset cycles. With increasing negative voltage, an unexpected negative set occurred at –2.5 V (state j), and the current reached $-I_{comp}$. As a result of this current jump, the CF began

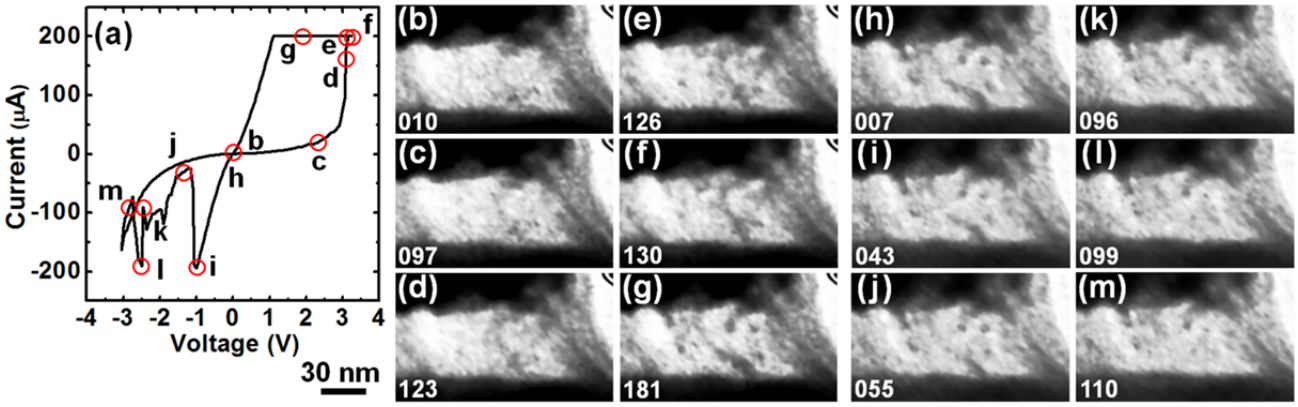

Fig. 11 (Example 2) First set/reset cycle with I_{comp} = 200 μA. (a) *I-V* switching curve and corresponding TEM video images of (b–g) set and (h–m) reset. The dark regions at the top and bottom are the Cu and TiN electrodes, respectively. The number shown in each photograph is the frame number in the set or reset cycle (frame interval of 30 ms). The reset cycle started 5 min after the set cycle.

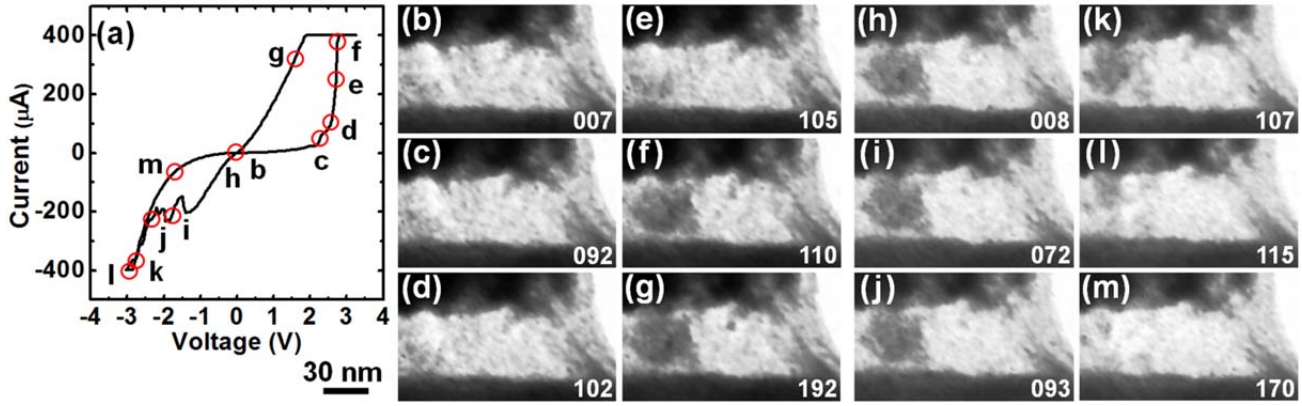

Fig. 12 (Example 2) The second set/reset cycle with I_{comp} = 400 μA. (a) *I-V* switching curve and corresponding TEM video images of (b–g) set and (h–m) reset. The dark regions at the top and bottom are the Cu and TiN electrodes, respectively. The number in each photograph is the frame number in the set or reset cycle (frame interval of 30 ms). The reset cycle started 5 min after the set cycle.

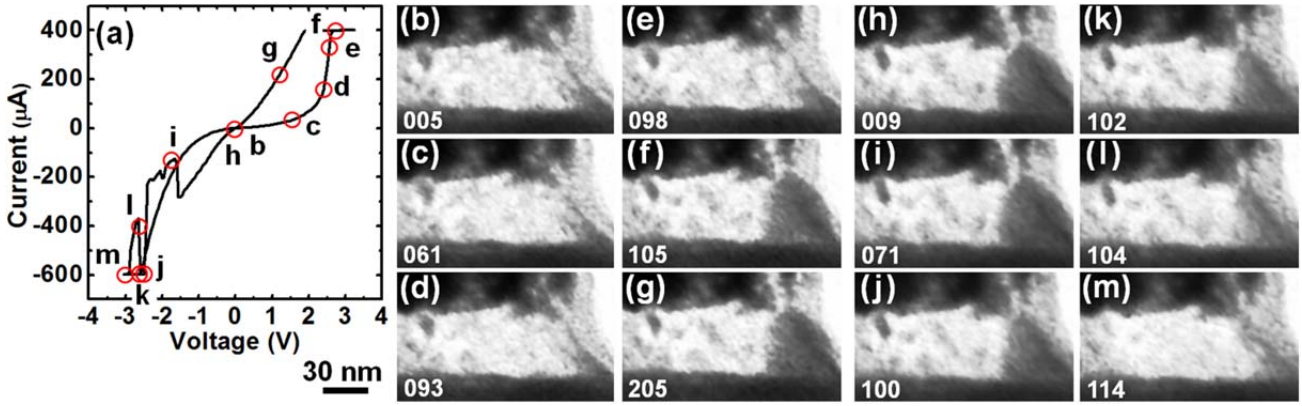

Fig. 13 (Example 2) The third set/reset cycle with I_{comp} = 400 μA. (a) *I-V* switching curve and corresponding TEM video images of (b–g) set and (h–m) reset. The dark regions at the top and bottom are the Cu and TiN electrodes, respectively. The number in each photograph is the frame number in the set or reset cycle (frame interval of 30 ms). The reset cycle started 5 min after the set cycle.

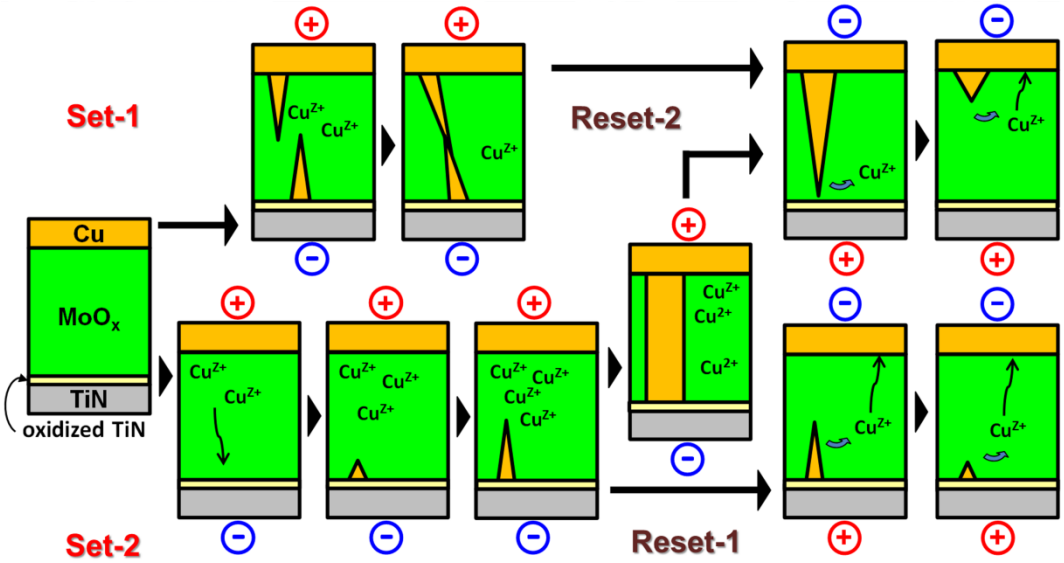

Fig. 14 Schematic of the filament transition process during ReRAM operation. There are two set modes and two reset modes.

to change in shape (Fig. 13(j) and (k)). The CF became thinner and subsequently vanished from the TE to the BE during the over-reset process (Fig. 13(l) and (m)). However, dissolution of the Cu CF was seen not only at the CF tip. In addition, a small precipitate located near the TE on the left also vanished between Fig. 13(l) and (m). The current flow was believed to be widely spread and thus contributed to the erasure of the CF and the nearby precipitate.

While we think the amorphous state of MoO_x was kept during the switching cycles, one may expect recrystallization of MoO_x near the switching position, because higher power was injected during the over-set/over-reset processes. Assuming MoO_2 conductive nanocrystals were formed, which cannot be identified in videos, the preferable switching position must be fixed there. This does not fit to the results in Figs. 11-13. On the other hand, if insulating MoO_3 nanocrystals were formed, the ionic conductivity could be reduced as discussed previously.[31] Though further investigation will be required for more detailed understanding, the discussion below will not be failed in this case.

Switching schemes

To summarize the experimental results described above, the set and reset operations are classified as shown in Fig. 14. There are two operating modes in the set process. When the MoO_x layer contains few Cu inclusions, a high set voltage is required. And, at this set switching, the Cu of the TE moves quickly into the MoO_x layer and generates deposits in the wider areas, and these deposits corrugate to form the CF. This is Set-1, as observed in Fig. 11. When a great deal of Cu is dissolved into the MoO_x layer in the initial state or during *I-V* repetition, however, the Cu deposit then appears at the interface with the BE. This deposit subsequently grows towards the TE and contributes to the CF. This is Set-2, which fits the behaviour of the conventional electrochemical model.[6,8,12,13] However, for realizing enough resistance reduction, the CF that connects the TE and the BE is not necessarily required. When there are sufficient Cu ions in the MoO_x layer, these ions may contribute the current between the CF and the TE. However, it cannot explain the result in Fig. 8(b)-(g). In previous works of other CBRAMs, the ionic state of Cu was reported Cu^{z+} (z = 1, 2).[64,65] Assuming that the CF is composed of fcc Cu, the CF should grow much larger than μm in the set process of Fig. 8(a), as measured over 4.5 s, if the current was contributed solely by this ionic current. There is a report that MoO_x can work as the VCM-type ReRAM.[30] Other factors, such as oxygen vacancies and electrons, should also contribute to the total current. Connection between the TE and the BE can be achieved with sufficient over-set processes. Yang et al.[35] investigated oxides with different Ag ion mobilities, and reported that Ag ions that were ionized at the Ag-oxide interface received electrons before drifting for long distances, and were reduced to form metallic Ag particles near this interface when the Ag mobility in the oxide is low compared with the reduction rate. The formed particles can work as bipolar electrodes and move towards the BE when a positive voltage is applied to the Ag (TE). When particle formation and movement occurs explosively, the CF can be seen to grow from the TE to the BE. Set-1 in Fig. 14 is categorized as this type of switching mode. This type of set (or forming) process has been reported in ZrO_2, SiO_2 and WO_x.[49,50,55] In contrast, the CF formation at the MoO_x-BE interface can be discussed using an analogy to electroplating. If MoO_x contains sufficient numbers of Cu ions, those locating near the BE can quickly reach the BE and initiate the CF formation there through electrochemical reduction. During voltage application, of course, oxidation of Cu(TE) should continue to maintain the current flow and the CF growth toward the TE from the BE. This is a plausible explanation for Set-2. A similar discussion was conducted based on the shape of the *I-V* curve in a previous report.[66]

There are two reset modes. When the CF does not bind the TE and the BE, the CF becomes thin overall and tends to shrink towards the BE. As shown in Fig. 13(h)–(m), the Cu of the CF

moves towards the TE. This is Reset-1, as listed in Fig. 14. In this case, the CF acts as the anode in the reset process under application of a negative voltage to the TE. Thus, the basics of this CF transition can be explained using the conventional filament model, where the Cu CF is electrochemically dissolved into the MoO_x layer and moves towards the TE, resulting in filament shrinkage. As shown in Fig. 3, the Cu does tend to be dissolved into the MoO_x even without voltage application. This tendency is thought to be enhanced with increasing temperature, as in other chemical reactions. The over-reset processes with high current may generate Joule heat (probably mainly at the CF), and the Cu dissolution can be enhance in the wider area of the CF. In contrast, when the CF bridges the TE and the BE, the CF ruptures in a region that is in contact with the BE (Reset-2). This is caused by the thin ox-TiN layer that is formed on the TiN BE, as discussed in our previous work.[53] The Joule heat is preferably generated near the bottom interface of the CF because the resistance of the ox-TiN layer is higher than that of the other regions. Therefore, the Cu of the lower part of the CF must preferably be dissolved into the MoO_x, and these dissolved Cu ions move along the widely spread electric field. In both Reset-1 and Reset-2, the heat generated in the CF is believed to play an important role in the CF shrinkage and erasure, in addition to the electrochemical processes. Widespread current leakage in the MoO_x layer is also an important factor in the reset process.

Strictly speaking, the above discussions based on Fig. 14 address CF formation/shrinkage in MoO_x during the over-set/over-reset processes. Sharp resistance switching in stable *I-V* cycles (e.g., as shown in Fig. 9) occurs without such large changes occurring in the CF microstructure in the MoO_x layer. Even in the *I-V* cycle where the CF showed a remarkable change in its microstructure, this change did not occur at the moment of set/reset switching. Therefore, stable switching is thought to be achieved in very localised regions of the CF. In our previous report, we claimed the contribution of a fine CF in a thin ox-TiN (i.e., TiO_2-like) layer on the TiN BE.[56] A similar phenomenon is believed to occur in the two examples that are discussed in this report, although the microstructural evolution of the ox-TiN layer could not be clearly detected in this work. This device structure can be classified as a CBRAM that is composed of a solid electrolyte layer and a thin oxide layer (i.e., a CBRAM with double switching layers), as in earlier works that showed stable ReRAM switching.[19,62,67,68] The thick CF (including the Cu deposit) in the solid electrolyte layer acts as a narrow TE that limits the actual device size (i.e., the switching region), while the repetition of the sharp switching is thought to occur because of the thin CF in the oxide. To realize stable switching cycles, it is important to control the power such that it does not erase the thick CF in the solid electrolyte layer.

Methods

Film preparation and characterization of MoO_x

Prior to the ReRAM experiments, the MoO_x film was characterized. The film was prepared by reactive radio-frequency (RF) sputtering of metallic Mo in an Ar-O_2 (20%) atmosphere at room temperature (RT) on SiO_2/Si, Si_3N_4/Si or Si substrates. The film was deposited using a Canon-Anelva E-200S (Kawasaki, Japan), where the base pressure was better than 4×10^{-4} Pa, the gas pressure was 1 Pa, and the RF power was 100 W. These deposition conditions were also used for all RF deposition processes in device fabrication and TEM sample preparation. The film thickness was 100, 50 or 30 nm, depending on the intended purpose of the film. The chemical state of the film was investigated by X-ray photoelectron spectroscopy (XPS) using the Shimadzu ESCA-3400 (Mg-Kα, 10 kV, 20 mA) (Kyoto, Japan). The wide-scan and narrow-scan spectra were measured with resolutions of 1 eV and 0.1 eV, respectively. The peak positions were corrected relative to the C 1s peak (284.6 eV) of the surface contaminant. Peak analyses were carried out using XPSpeak41.[69] For the spectrum analysis, Gaussian-Lorentzian peak functions and a Shirley-type background function were assumed. The crystal structure was checked by X-ray diffractometry (XRD) using the Rigaku RU-300 (Cu-Kα, 50 kV, 260 mA) (Akishima, Japan). Scanning electron microscopy (SEM) was also performed to observe the film morphology using a Hitachi S-4800 FE-SEM (field-emission SEM) (Tokyo, Japan) that operated at 5 kV. TEM was also used to observe the dissolution of Cu into the MoO_x layer.

Device fabrication and ReRAM measurements

The ReRAM had a Pt/Cu/MoO_x/TiN structure, where Pt/Cu and TiN were the top and bottom electrodes (TE and BE), respectively. After the deposition of TiN (100-nm-thick) on a SiO_2/Si(001) wafer by RF reactive sputtering of metallic Ti under an Ar-20%N_2 atmosphere, a SiO_2 (300-nm-thick) insulating layer was deposited by RF sputtering. Subsequently, circular contact holes (ranging from several μm to several tens of μm in diameter) were fabricated using a combination of photolithography followed by reactive ion etching (RIE). After patterning, which was followed by O_2-plasma cleaning, MoO_x (50-nm-thick), Cu (30-nm-thick) and Pt (100-nm-thick) layers were deposited without breaking the vacuum. The ReRAM properties were then investigated by performing *I-V* measurements and pulse switching, during which the Pt/Cu TE was biased. All measurements were performed in air at RT using a Yokogawa GS610 source-measure-unit (SMU) (Musashino, Japan).

In situ TEM experiments

The Pt/Cu/MoO_x tri-layer film was formed on a TiN/Si(001) wafer, where the TiN surface was pre-treated by O_2-plasma cleaning prior to the film deposition. The film was prepared using the processes described above. After the wafer was cut into smaller pieces (2.5 mm × 100 μm × 525 μm), the in situ TEM samples were prepared using the ion-shadow method, which is a type of ion milling process.[70,71] The samples were set in a specially-designed home-made TEM holder system containing a piezo actuator,[61] and the *I-V* curves were

measured with simultaneous image recording at a video frame rate of 30 frames s^{-1}. The electron microscope was the Jeol JEM2010 (C_s = 0.5 mm) (Akishima, Japan) and operated at 200 kV. The electrical measurements were performed using the Yokogawa GS820 SMU (Musashino, Japan), where the Pt/Cu TE was biased and the TiN/Si BE was grounded. The voltage sweep rate was in the 0.3–1.6 V/s range, and no clear differences in the *I-V* curve were seen to depend on the sweep rate. The electronic measurements were carried out through Si. Therefore, the current in the LRS was limited by this serially connected resistance of TiN/Si. The image contrast of the video was enhanced nonlinearly to enable clear identification of the faint contrast in the switching layer. In addition, frame averaging was used to reduce the overall noise. The image processing was performed using home-made software and commercially available hardware. The processed videos are shown in the supplementary information files (ESI_1.wmv and ESI_2.wmv), where the frame rate is accelerated by four times.

Conclusions

The set/reset processing of the Cu/MoO_x/ox-TiN/TiN (or Cu/Cu:MoO_x/ox-TiN/TiN) ReRAM was investigated using in situ TEM. The growth/shrinkage of the CF in the over-set/over-reset processes can be classified into two set modes and two reset modes. The appearance of each of these switching modes is dependent on the switching history of the CBRAM, e.g., the amount of Cu inclusions in the MoO_x layer and the geometry of the CF before the switching process. To produce an observable change in the CF geometry in the MoO_x layer, a high current (and thus sufficient Joule heating) is required. However, sharp and stable switching can be achieved without the need for such major changes, and the local region of the CF is thought to contribute to the ReRAM switching, which probably involves formation of a thin CF in the ox-TiN layer. Stable ReRAM switching with high performance has been reported on double layered CBRAMs, such as Cu-Te/oxide[19] and Cu:MoO_x/GdO_x configurations.[62] A combination of a solid electrolyte with high levels of Cu inclusions and an oxide with reduced solubility is thought to be most effective. Similar double layer structures were also used for VCM-type ReRAMs,[72-74] where the oxygen vacancies form the CF. Kudo et al. investigated a miniaturized Cu-Te/insulator device using in situ TEM, and claimed the formation of Cu filament in nanometre scale.[54] For further analysis of this type of CBRAM operation, nanometre-scale or sub-nanometre scale observations of the CF in the ox-TiN layer using an in situ TEM will be required. As described above in "Characterization of MoO_x film" section, our MoO_x prepared by reactive sputtering showed high Cu solubility, and smooth Cu movement was seen in Fig. 12. This may be one of the reasons that we succeeded to realize smooth switching cycles without device destruction caused by strong current overshoot in the set process. On the other hand, this character may induce short LRS retention time and HRS failure, because Cu of the CF and the TE can move into the MoO_x layer. Further optimization of device structure should be carefully performed to realize realistic and stable ReRAM devices. MoO_x seem to have intermediate characteristics as a solid electrolyte between GeS (or chalcogenides) and Ta_2O_5 (or SiO_2) which have been investigated for CBRAMs. Results obtained in this work will give important information to understand operation details in these CBRAMs.

Acknowledgements

This work was supported by the KAKENHI program of the Japan Society for the Promotion of Science (JSPS) (Grant Nos 25420279, 26630141, and 15H01706). The work was also supported by the Mitsubishi Foundation, the Nippon Sheet Glass Foundation for Materials Science and Engineering, and the Scholar Project of the Toyota Physical and Chemical Research Institute. Some of the experiments were conducted as part of the Nanotechnology Platform Program and the Cooperative Research Program of the Network Joint Research Center for Materials and Devices, both of which were organized by the Ministry of Education, Culture, Sports, Science and Technology (MEXT), Japan. The XRD experiment was carried out at the High Brilliance X-ray Laboratory at Hokkaido University.

References

1 M. N. Kozicki, M. Yun, L. Hilt and A. Sing, in *Proc. Solid-State Ionic Devices: 195th Electrochem. Soc. Proc.*, Vol. 99-13, ed. E. D Wachsman, J. R. Akridge, M. Liu and N. Yamazoe, Electrochem. Soc., Pennington, 1999, pp. 298–309.
2 S. Q. Liu, N. J. Wu and A. Ignatiev, *Appl. Phys. Lett.*, 2000, **76**, 2749–2751.
3 S. Seo, M. J. Lee, D. H. Seo, E. J. Jeoung, D.-S. Suh, Y. S. Joung, I. K. Yoo, I. R. Hwang, S. H. Kim, I. S. Byun, J.-S. Kim, J. S. Choi and B. H. Park, *Appl. Phys. Lett.*, 2004, **85**, 5655–5657.
4 R. Waser and M. Aono, *Nat. Mater.*, 2007, **6**, 833–840.
5 A. Sawa, *Mater. Today*, 2008, **11**, 28–36.
6 R. Waser, R. Dittmann, G. Staikov and K. Szot, *Adv. Mater.*, 2009, **21**, 2632–2663.
7 H. Akinaga and H. Shima, *Proc. IEEE*, 2010, **98**, 2237–2251.
8 A. Chen, *Ionic Memory Technology*, in *Solid State Electrochemistry II: Electrodes, Interfaces and Ceramic Membranes*, V. V. Kharton, Wiley-VCH, Weinheim, 1st ed., 2011, pp.1–30, doi: 10.1002/9783527635566.ch1.
9 K. M. Kim and C. S. Hwang, *Nanotechnology*, 2011, **22**, 254002.
10 Y. Yang and W. Lu, *Nanoscale*, 2013, **5**, 10076–10092.
11 P. R. Mickel, A. J. Lohn and M. J. Marinella, Modern Phys. Lett. B, 2014, **28**, 1430003.
12 F. Pan, S. Gao, C. Chen, C. Song and F. Zeng, *Mater. Sci. Eng. R*, 2014, **83**, 1–59.
13 L. Goux and I. Valov, *Phys. Stat. Solidi A*, 2016, **213**, 274–288.
14 T. Chang, S.-H. Jo, K.-H. Kim, P. Sheridan, S. Gaba and W. Lu, *Appl. Phys. A*, 2011, **102**, 857–863.
15 D. S. Jeong, I. Kim, M. Ziegler and H. Kohlstedt, *RSC Adv.*, 2013, **3**, 3169-3183.
16 M. Prezioso, F. Merrikh-Bayat, B. D. Hoskins, G. C. Adam, K. K. Likharev and D. B. Strukov, *Nature*, 2015, **521**, 61–64.
17 B. DeSalvo, E. Vianello, D. Garbin, O. Bichler and L.Perniola, in *Proc. 7th Internat. Memory Workshop (IMW)*, IEEE, Piscataway, 2015, pp. 9–12. doi: 10.1109/IMW.2015.7150286

18 M. N. Kozicki, M. Park and M. Mitkova, *IEEE Trans. Nanotechnology*, 2005, **4**, 331–338.
19 K. Aratani, K. Ohba, T. Mizuguchi, S. Yasuda, T. Shiimoto, T. Tsushima, T. Sone, K. Endo, A. Kouchiyama, S. Sasaki, A. Maesaka, N. Yamada and H. Narisawa, *Tech. Dig. Int. Electron Devices Meet.*, 2007, 783–786. doi: 10.1109/IEDM.2007.4419064
20 M. N. Kozicki, C. Gopalan, M. Balakrishnan and M. Mitkova, *IEEE Trans. Nanotechnology*, 2006, **5**, 535–544.
21 C. Kügeler, R. Rosezin, R. Weng, R. Waser, S. Menzel, B. Klopstra and U. Böttger, in *Proc. 9th Nanotechnology Conf.: IEEE NANO 2009*, IEEE, Piscataway, 2009, pp. 1102‑1105.
22 C. Schindler, M. Weides, M. N. Kozicki and R. Waser, *Appl. Phys. Lett.*, 2008, **92**, 122910.
23 C.-Y. Liu and P.-W. Sung, *Japn. J. Appl. Phys.*, 2011, **50**, 091101.
24 Y. Bernard, V. T. Renard, P. Gonon and V. Jousseaume, *Microelect. Eng.*, 2011, **88**, 814–816.
25 M. Haemori, T. Nagata and T. Chikyow, *Appl. Phys. Exp.*, 2009, **2**, 061401.
26 T. Sakamoto, K. Lister, N. Banno, T. Hasegawa, K. Terabe and M. Aono, *Appl. Phys. Lett.*, 2007, **91**, 092110.
27 A. Sleiman, P. W. Sayers and M. F. Mabrook, *J. Appl. Phys.*, 2013, **113**, 164506.
28 S. Z. Rahaman, S. Maikap, W. S. Chen, H. Y. Lee, F. T. Chen, M. J. Kao and M. J. Tsai, *Appl. Phys. Lett.*, 2012, **101**, 073106.
29 D. Lee, D. Seong, I. Jo, F. Xiang, R. Dong, S. Oh and H. Hwang, *Appl. Phys. Lett.*, 2007, **90**, 122104.
30 M. Arita, H. Kaji, T. Fujii and Y. Takahashi, *Thin Solid Films*, 2012, **520**, 4762–4767.
31 T. Tsuruoka, K. Terabe, T. Hasegawa and M. Aono, *Nanotechnology*, 2010, **21**, 425205.
32 M. A. Villena, F. Jiménez-Molinos, J. B. Roldán, J. Suñé, S. Long, X. Lian, F. Gámiz and M. Liu, *J. Appl. Phys.*, 2013, **114**, 144505.
33 D. Ielmini, *IEEE Trans. Electron Devices*, 2011, **58**, 4309–4317.
34 T. Tsuruoka, K. Terabe, T. Hasegawa, I. Valov, R. Waser and M. Aono, *Adv. Funct. Mater.*, 2012, **22**, 70–77.
35 Y. Yang, P. Gao, L. Li, X. Pan, S. Tappertzhofen, S. Choi, R. Waser, I. Valov and W. D. Lu, *Nat. Commun.*, 2014, **5**, 4232.
36 X. Tian, S. Yang, M. Zeng, L. Wang, J. Wei, Z. Xu, W. Wang, and X. Bai, *Adv. Mater.*, 2014, **26**, 3649–3654.
37 Ch. Jooss, J. Hoffmann, J. Fladerer, M. Ehrhardt, T. Beetz, L. Wu and Y. Zhu, *Phys. Rev. B.*, 2008, **77**, 132409.
38 T. Fujii, H. Kaji, H. Kondo, K. Hamada, M. Arita and Y. Takahashi, *IOP Conf. Ser.: Mater. Sci. Eng.*, 2010, **8**, 012033.
39 Y. Yang, W. Lu, Y. Yao, J. Sun, C. Gu, L. Gu, Y. Wang, X. Duan and R. Yu, *Scientific Reports*, 2014, **4**, 3890.
40 D.-H. Kwon, K. M. Kim, J. H. Jang, J. M. Jeon, M. H. Lee, G. H. Kim, X.-S. Li, G.-S. Park, B. Lee, S. Han, M. Kim and C. S. Hwang, *Nat. Nanotechnol.*, 2010, **5**, 148–153.
41 T. Fujii, M. Arita, K. Hamada, H. Kondo, H. Kaji, Y. Takahashi, M. Moniwa, I. Fujiwara, T. Yamaguchi,M. Aoki, Y. Maeno, T. Kobayashi and M. Yoshimaru, *J. Appl. Phys.*, 2011, **109**, 053702.
42 J.-Y. Chen, C.-L. Hsin, C.-W. Huang, C.-H. Chiu, Y.-T. Huang, S.-J. Lin, W.-W. Wu and L.-J. Chen, *Nano Lett.*, 2013, **13**, 3671–3677.
43 G.-S. Park, Y. B. Kim, S. Y. Park, X. S. Li, S. Heo, M.-J. Lee, M. Chang, J. H. Kwon, M. Kim, U.-I. Chung, R. Dittmann, R. Waser and K. Kim, *Nat. Commun.*, 2013, **4**, 2382.
44 T. Fujii, M. Arita, K. Hamada, Y. Takahashi and N. Sakaguchi, *J. Appl. Phys.*, 2013, **113**, 083701.
45 Z. Fan, X. Fan, A. Lic and L. Dong, *Nanoscale*, 2013, **5**, 12310–12315.
46 K. D'Aquila, Y. Liu, H. Iddir and A. K. Petford-Long, *Phys. Stat. Solidi RRL*, 2015, **9**, 301–306.
47 T. Fujii, M. Arita, Y. Takahashi and I. Fujiwara, *Appl. Phys. Lett.*, 2011, **98**, 212104.
48 S.-J. Choi, G.-S. Park, K.-H. Kim, S. Cho, W.-Y. Yang, X.-S. Li, J.-H. Moon, K.-J. Lee and K. Kim, *Adv. Mater.*, 2011, **23**, 3272–3277.
49 Y. Yang, P. Gao, S. Gaba, T. Chang, X. Pan and W. Lu, *Nat. Commun.*, 2012, **3**, 732.
50 Q. Liu, J. Sun, H. Lv, S. Long, K. Yin, N. Wan, Y. Li, L. Sun and M. Liu, *Adv. Mater.*, 2012, **24**, 1844–1849.
51 T. Fujii, M. Arita, Y. Takahashi and I. Fujiwara, *J. Mater. Res.*, 2012, **27**, 886–896.
52 J. Sun, Q. Liu, H. Xie, X. Wu, F. Xu, T. Xu, S. Long, H. Lv, Y. Li, L. Sun and M. Liu, *Appl. Phys. Lett.*, 2013, **102**, 053502.
53 M. Kudo, M. Arita, Y. Ohno and Y. Takahashi, *Appl. Phys. Lett.*, 2014, **105**, 173504.
54 M. Kudo, M. Arita, Y. Takahashi, K. Ohba, M. Shimuta and I. Fujiwara, in *Proc. 7th Internat. Memory Workshop (IMW)*, IEEE, Piscataway, 2015, pp. 85–88. doi: 10.1109/IMW.2015.7150312
55 M. Arita, A. Takahashi, Y. Ohno, A. Nakane, A. Tsurumaki-Fukuchi and Y. Takahashi, *Scientific Reports*, 2015, **5**, 17103.
56 M. Arita, Y. Ohno and Y. Takahashi, *Phys. Stat. Solidi A*, 2016, **213**, 306–310.
57 ed. C. D. Wagner, W. M. Riggs, L. E. Davis, J. F. Moulder and G. E. Muilenberg, *Handbook of X-ray Photoelectron Spectroscopy*, Perkin-Elmer Corp., Eden Pralrie, 1979.
58 National Institute of Standards and Technology (NIST) Online, http://srdata.nist.gov/xps/ElmComposition.aspx, (accessed April 2013).
59 J.-G. Choi and L. T. Thompson, *Appl. Surf. Sci.*, 1993, **93**, 143–149.
60 W.-C. Chang, X. Qi, J.-C. Kuo, S. Lee, S.-K. Ng and D. Chen, *Cryst. Eng. Comm.*, 2011, 13, 5125–5132.
61 M. Arita, K. Hamada, Y. Takahashi, K. Sueoka and T. Shibayama, *In Situ Transmission Electron Microscopy for Electronics*, in *Transmission Electron Microscope*, ed. M. Khan, InTech, Rijeka, 2015, Chap. 2, pp. 35–68. doi: 10.5772/ 60651
62 J. Yoon, H. Choi, D. Lee, J.-B. Park, J. Lee, D.-J. Seong, Y. Ju, M. Chang and H. Hwang, *IEEE Electro. Dev. Lett.*, 2009, **30**, 457–459.
63 S. P. Thermadam, S. K. Bhagat, T. L. Alford, Y. Sakaguchi, M. N. Kozicki and M. Mitkova, *Thin Solid Films*, 2010, **518**, 3293–3298.
64 S. Tappertzhofen, H. Mündelein, I. Valov and R. Waser, *Nanoscale*, 2012, **4**, 3040–3043.
65 T. Tsuruoka, I. Valov, S. Tappertzhofen, J. van den Hurk, T. Hasegawa, R. Waser and M. Aono, *Adv. Funct. Mater.*, 2015, **25**, 6374–6381.
66 F. Zhuge, K. Li, B. Fu, H. Zhang, J. Li, H. Chen, L. Liang, J. Gao, H. Cao, Z. Liu and H. Luo, *AIP Adv.*, 2015, **5**, 057125.
67 M. Tada, T. Sakamoto, N. Banno, M. Aono, H. Hada and N. Kasai, *IEEE Trans. Electron Devices*, 2010, **57**, 1987–1995.
68 S. Z. Rahaman, S. Maikap, W. S. Chen, H. Y. Lee, F. T. Chen, T. C. Tien and M. J. Tsai, *J. Appl. Phys.*, 2012, **111**, 063710.
69 R. Kwok, XPSpeak4.1, Chin. Univ. Hong Kong, Shatin, 1998.
70 R. Hirose, M. Arita, K. Hamada and A. Okada, *Mater. Sci. Eng. C*, 2003, **23**, 927–930.
71 M. Kudo, M. Arita, Y. Ohno, T. Fujii, K. Hamada, Y. Takahashi, *Thin Solid Films*, 2013, **533**, 48–53.
72 M.-J. Lee, C. B. Lee, D. Lee, S. R. Lee, M. Chang, J. H. Hur, Y.-B. Kim, C.-J. Kim, D. H. Seo, S. Seo, U. Chung, I.-K. Yoo and K. Kim, *Nat. Mater.*, 2011, **10**, 625–630.
73 J. P. Strachan, J. J. Yang, L. A. Montoro, C. A. Ospina, A. J. Ramirez, A. L. D. Kilcoyne, G. Medeiros-Ribeiro and R. S. Williams, *Beilstein J. Nanotechnol.*, 2013, **4**, 467–473.
74 Q. Wang, Y. Itoh, T. Tsuruoka, S. Ohtsuka, T. Shimizu, S. Shingubara, T. Hasegawa and M. Aono, *Phys. Stat. Solidi RRL*, 2015, **9**, 166–170.

